



## Distance-Dependent Fluorescence Quenching of *p*-Bis[2-(5-phenyloxazolyl)]benzene by Various Quenchers

Bogumil Zelent,<sup>†</sup> Józef Kuśba,<sup>§</sup> Ignacy Gryczynski,<sup>†</sup> Michael L. Johnson,<sup>‡</sup> and Joseph R. Lakowicz<sup>\*,†</sup>

Center for Fluorescence Spectroscopy, Department of Biological Chemistry, and Medical Biotechnology Center, University of Maryland at Baltimore, School of Medicine, 108 N. Greene Street, Baltimore, Maryland 21201, Department of Pharmacology, Box 448, Jordan Hall, Room 561, University of Virginia, Charlottesville, Virginia 22908, and Faculty of Applied Physics and Mathematics, Technical University of Gdańsk, ul. Narutowicza 11/12, 80-952 Gdańsk, Poland

Received: June 24, 1996; In Final Form: September 19, 1996<sup>®</sup>

We report results of frequency-domain and steady-state measurements of the fluorescence quenching of *p*-bis[2-(5-phenyloxazolyl)]benzene (POPOP) when quenched by bromoform (CHBr<sub>3</sub>), methyl iodide (CH<sub>3</sub>I), potassium iodide (KI), 1,2,4-trimethoxybenzene (TMB), or *N,N*-diethylaniline (DEA). The quenching efficiency of these compounds decreased in the order DEA, TMB, KI, CH<sub>3</sub>I, CHBr<sub>3</sub>. In the case of DEA and TMB the measurements clearly confirm the applicability of the exponential distance-dependent quenching (DDQ) model, in which the bimolecular quenching rate  $k(r)$  depends exponentially on the fluorophore–quencher separation  $r$ ,  $k(r) = k_a \exp[-(r - a)/r_c]$ , where  $a$  is the distance of closest approach. Simultaneous analysis of the frequency-domain and steady-state data significantly improved resolution of the recovered molecular parameters  $k_a$  and  $r_c$ . The data for DEA and TMB cannot be satisfactorily fit using either the Smoluchowski or Collins–Kimball radiation boundary condition (RBC) model. The quenching behavior of the less efficient quenchers KI, CH<sub>3</sub>I, and CHBr<sub>3</sub> can be adequately described with both the DDQ and RBC models, but this may be a simple consequence of less efficient quenching. The efficiency of quenching is discussed on the basis of the mechanisms of interaction between the fluorophore and quencher molecules, which involves electron transfer and/or heavy atom effects.

### Introduction

Collisional quenching of fluorescence has been widely used in physical chemistry and biochemistry. Fluorescence quenching of aromatic and heteroaromatic hydrocarbons by aromatic amines,<sup>1–13</sup> aromatic nitriles,<sup>14</sup> haloalkanes,<sup>15–24</sup> and halide ions<sup>25–27</sup> as well as by nitroxides<sup>28,29</sup> and oxygen<sup>30,31</sup> has been studied to determine the bimolecular rate constants, to characterize the solvent effects on quenching, and to determine the mechanisms of interaction between the fluorophore and quencher molecules. Moreover, collisional quenching of tryptophan fluorescence by a variety of ionic and neutral quenchers has been used to study the structure and dynamics of proteins<sup>32–40</sup> and membranes.<sup>41,42</sup> Collisional or dynamic quenching requires contact between the fluorophore and quencher molecules during the lifetime of the excited state. The quenching data can reveal information about accessibility of fluorophores in macromolecules to externally added quenchers and the diffusion of quenchers within proteins and membranes.

For many fluorophores in solution, including aromatic and heteroaromatic fluorophores, the intensity decays are often monoexponential.<sup>43</sup> However, in the presence of collisional quenching the monoexponential intensity decays become nonexponential due to transient effects in diffusion.<sup>21,44–46</sup> This effect in collisional quenching of fluorescence is due to a rapid decay of closely spaced fluorophore–quencher pairs, followed by slower diffusion-limited quenching of remaining fluorophores. These effects can be readily detected by using

frequency-domain fluorometry.<sup>47–49</sup> We have shown for several fluorophore–quencher systems that analysis of the frequency-domain data can recover diffusion coefficients, interaction radii, and specific rate constants for quenching.<sup>50–52</sup>

Interpretation of collisional quenching data is usually based on the theory of the Smoluchowski<sup>53</sup> or Collins–Kimball radiation boundary condition (RBC)<sup>54,55</sup> models. The theory of Smoluchowski assumes that the quenching occurs only during the direct contact of the fluorophore with the quencher, and upon contact the fluorophore instantaneously returns to the ground state. This model of quenching involves a transient term due to diffusion, which results in nonexponential intensity decays. The RBC model also assumes that the quenching occurs only during the direct contact of the fluorophore with the quencher, but does not assume instantaneous quenching upon contact (Scheme 1). The RBC model predicts the finite (specific) rate constant ( $\kappa$ ) for quenching. The quenching rate  $k(r)$  assumes the value of  $\kappa\delta(r - a)$  at the encounter distance of the closest approach  $a$ , where  $\delta(r - a)$  is a Dirac delta. For the case where  $\kappa \rightarrow \infty$  the RBC model becomes equivalent to the Smoluchowski model.

Our recent results on collisional quenching of *p*-bis[2-(5-phenyloxazolyl)]benzene (POPOP) by carbon tetrabromide,<sup>50</sup> anthracenes by *N,N*-diethylaniline,<sup>52</sup> and *N*-acetyl-L-tryptophanamide by acrylamide<sup>51</sup> revealed that the time-resolved data in the presence of collisional quenching could not be completely described by the RBC model. These data indicated the need for a distance-dependent rate of quenching (DDQ) to explain the experimental data. The two models for collisional quenching of fluorescence are compared in Scheme 1. For the RBC model  $k(r) = 0$  when  $r > a$ , and the rate of quenching is described by the interaction of the fluorophore–quencher at the contact

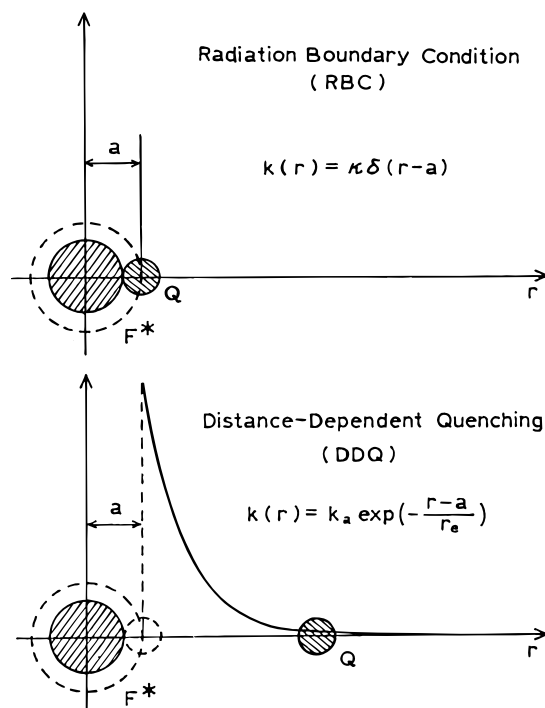
\* Corresponding author.

<sup>†</sup> University of Maryland at Baltimore.

<sup>‡</sup> University of Virginia.

<sup>§</sup> Technical University of Gdańsk.

<sup>®</sup> Abstract published in *Advance ACS Abstracts*, November 1, 1996.

**SCHEME 1: Comparison of the RBC and DDQ Models for Collisional Quenching of Fluorescence**

distance  $a$ . The DDQ model assumes that the rate of quenching  $k(r)$  is exponentially dependent on the fluorophore–quencher distance and is given by the expression<sup>56,57</sup>

$$k(r) = k_a \exp[-(r-a)/r_e] \quad (1)$$

where  $k_a$  is the value of  $k(r)$  at the encounter distance  $r = a$ ,  $a$  is the distance of closest approach, and  $r_e$  is the characteristic parameter of the interaction that defines the decrease of  $k(r)$  with distance.

To obtain mechanistic insight into the nature of collisional quenching, we chose to examine the fluorophore POPOP when quenched by  $\text{CHBr}_3$ ,  $\text{CH}_3\text{I}$ , KI, 1,2,4-trimethoxybenzene (TMB), and *N,N*-diethylaniline (DEA). POPOP was chosen for its short decay time near 1.3 ns in the absence of quenching. The nanosecond decay time of POPOP is valuable because the transient effects mostly occur on the subnanosecond time scale and are less apparent for longer decay times. Since the transient effects are less apparent at higher rates of diffusion, we used propylene glycol as the solvent to provide moderate viscosities that still allow diffusive quenching with reasonable amounts of quenching and readily apparent transient effects. Additionally, POPOP displays a single-exponential decay in most solvents, allowing the transient effects to be seen as deviations from the single-exponential model.

The quenchers were selected with the expectation that the mechanism of quenching would change across the series. In particular, we expected heavy atom interactions to occur for  $\text{CHBr}_3$  and  $\text{CH}_3\text{I}$  and electron transfer to occur for TMB and DEA. In the case of KI the quenching could be due to either mechanism. The Förster energy transfer is not expected to occur from POPOP to any of these quenchers. By examination of this series of quenchers we hoped to be able to determine how the mechanism of interaction is reflected in the recovered values of  $k_a$ ,  $a$ , and  $r_e$  (eq 1).

**Materials and Methods**

*p*-Bis[2-(5-phenyloxazolyl)]benzene (POPOP), anhydrous, was from Sigma Chemical Co., Inc. (St. Louis, MO). 1,2,4-

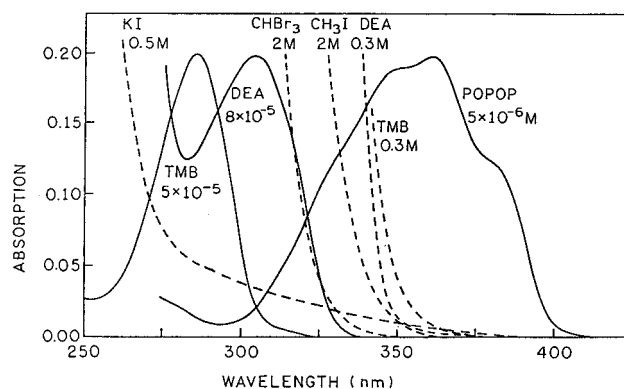


**Figure 1.** Absorption spectra of POPOP ( $5 \times 10^{-6}$  M), 1,2,4-trimethoxybenzene (0.3 and  $5 \times 10^{-5}$  M), *N,N*-diethylaniline (0.3 and  $8 \times 10^{-5}$  M), bromoform (2 M), methyl iodide (2 M), and potassium iodide (0.5 M) in propylene glycol ( $d = 1$  cm).

Trimethoxybenzene (97%), bromoform (99+%), methyl iodide (99.5%), and potassium iodide were obtained from Aldrich Chemical Co., Inc. (Milwaukee, WI) and were used without further purification. *N,N*-Diethylaniline (p.a. grade), from Fluka Chemie A. G. (Switzerland), was purified by vacuum distillation in a grease-free, mercury-free vacuum line. The colorless liquid aromatic amine was stored under an oxygen-free nitrogen atmosphere in the dark. 1,2-Propanediol (propylene glycol) (p.a. grade) was from Janssen Chimica (Spectrum Chemical Mfg. Corp., Gardena, CA). The concentration of POPOP in the samples was  $5 \times 10^{-6}$  M, while that of *N,N*-diethylaniline and 1,2,4-trimethoxybenzene ranged from 0 to 0.3 M. *N,N*-Diethylaniline (0.3125 M) and 1,2,4-trimethoxybenzene (0.3125 M) in propylene glycol were purged by oxygen-free nitrogen gas and equilibrated for 24 h at room temperature in the dark in order to obtain the homogeneous stock solutions. The solutions of potassium iodide, bromoform, and methyl iodide in propylene glycol were prepared immediately before use.

Absorption spectra were measured on a Perkin-Elmer Lambda 6, UV/vis spectrophotometer (The Perkin-Elmer Corp., Rockville, MD). Steady-state fluorescence measurements were carried out using a SLM 8000 photon-counting spectrofluorometer (SLM Instruments, Inc., Urbana, IL) equipped with a thermostated cell holder.

Frequency-domain fluorescence measurements were performed using the frequency-domain fluorometer described previously in detail.<sup>47,48</sup> The modulated excitation was provided by the harmonic content of a laser pulse train with a repetition rate of 3.795 MHz and a pulse width about 7 ps, obtained from a synchronously pumped and cavity-dumped pyridine-2 dye laser. The light was frequency doubled to 370 nm. The dye laser was pumped with a mode-locked argon ion laser (Coherent, Innova 15). The emitted light was detected by using a microchannel plate photomultiplier tube (Hamamatsu R1564U), which was externally cross-correlated.<sup>48</sup> All intensity decays were measured by using rotation-free polarization conditions (magic-angle polarizer orientation) with the fluorophore emission selected by 3-74 and 7-59 (Corning) filters.

The theory for the intensity decays in the presence of distance-dependent quenching is presented in the Appendix.

**Results and Discussion**

*p*-Bis[2-(5-phenyloxazolyl)]benzene (POPOP) is a hetero-aromatic fluorophore that in propylene glycol possesses an absorption spectrum characterized by a weakly fine structured band between 300 and 400 nm (Figure 1). These absorption spectra show that POPOP in propylene glycol can be selectively

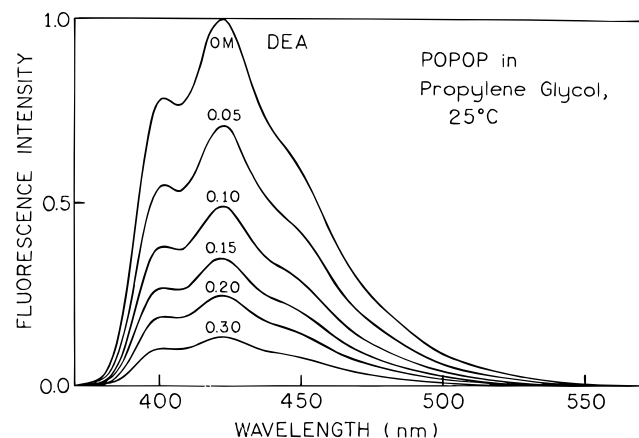


**Figure 2.** Fluorescence emission spectra of POPOP in propylene glycol at 25 °C ( $\lambda_{\text{exc}} = 370$  nm) in the presence of increasing concentrations of *N,N*-diethylaniline (0, 0.05, 0.10, 0.15, 0.20, and 0.30 M).

excited in the presence of 1,2,4-trimethoxybenzene (TMB), *N,N*-diethylaniline (DEA), methyl iodide ( $\text{CH}_3\text{I}$ ), bromoform ( $\text{CHBr}_3$ ), or potassium iodide (KI). The quenchers all absorb light at wavelengths significantly below the emission spectrum of POPOP (Figure 2), excluding the possibility of Förster transfer. The fluorescence emission of POPOP can be quenched by typical electron-donor molecules like aromatic amines<sup>5,13</sup> or methoxybenzenes. This quenching involves electron transfer and indicates the electron-acceptor character of POPOP molecule. Figure 2 shows the emission spectrum of POPOP in propylene glycol at 25 °C in the absence and presence of DEA. It is clearly seen that the fluorescence emission of POPOP with the maximum at 423 nm strongly decreases in intensity in the presence of increasing concentrations of DEA in solution. However, the observed quenching is not accompanied by the appearance of a new long wavelength emission. Similar results are also obtained for POPOP quenched by TMB. The absence of exciplex emission for POPOP–DEA as well as for POPOP–TMB in propylene glycol can be explained by a solvent polarity effect<sup>52</sup> or by a nonemissive exciplex.<sup>13</sup> Figure 2 also shows that the fine structure of the emission spectrum of POPOP does not change even in the presence of the highest concentrations of DEA (0.3 M), suggesting the absence of photodegradation products. Analogous behavior of the quenched spectral shapes was observed when TMB,  $\text{CH}_3\text{I}$ ,  $\text{CHBr}_3$ , and KI were used as quenchers. The electron transfer mechanism of quenching of singlet POPOP by DEA and TMB is due to the comparatively low ionization energy of DEA and TMB, with oxidation potentials of 0.76 and 1.12 V,<sup>4</sup> respectively. Iodide ion can act as an electron donor. POPOP is a good electron acceptor characterized by a redox potential of  $-1.77$  V.<sup>13</sup> On the basis of the polarographic oxidation and reduction potentials data presented in Table 1, we calculated the free energy  $\Delta G_{\text{ET}}$  of the electron transfer process in the POPOP–donor molecule systems using the Rehm and Weller<sup>4,5</sup> equation

$$\Delta G_{\text{ET}} = E_{1/2}^{\text{ox}}(\text{D/D}^+) - E_{1/2}^{\text{red}}(\text{A}^{\cdot-}/\text{A}) - E_s + C \quad (2)$$

where  $E_{1/2}^{\text{ox}}(\text{D/D}^+)$  refer to half-wave oxidation potential of the electron donor and  $E_{1/2}^{\text{red}}(\text{A}^{\cdot-}/\text{A})$  the reduction potential of the electron-acceptor molecules, respectively.  $E_s$  is the singlet excitation energy expressed as the 0–0 electronic transition of the fluorophore molecule, and  $C(\text{eV}) = e^2/\epsilon R 4\pi\epsilon_0$  is the Coulomb energy change associated with the charge separation distance  $R$ .<sup>62</sup> The negative values of  $\Delta G_{\text{ET}}$  (see Table 2) characterize the overall feasibility of the electron transfer quenching interactions.

**TABLE 1: Half-Wave Polarographic Oxidation and Reduction Potentials<sup>a</sup> and First Singlet Energy Levels for POPOP and Some Quencher Molecules**

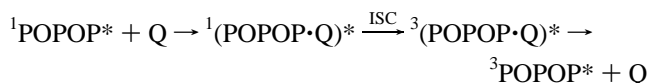
compound	$E_{1/2}^{\text{ox}}(\text{D/D}^+)$ [V]	$E_{1/2}^{\text{red}}(\text{A}^{\cdot-}/\text{A})$ [V]	$E_s$ [eV]
POPOP		$-1.77^c$	3.27
DEA	0.76 <sup>b</sup>		4.10
TMB	1.12 <sup>b</sup>		4.32
KI	0.9 <sup>e</sup>		
$\text{CBr}_4$		$-0.30^d$	
$\text{CHBr}_3$		$-0.64^d$	
$\text{CCl}_4$		$-0.78^d$	
$\text{CH}_3\text{I}$		$-1.63^d$	

<sup>a</sup> Measured versus saturated calomel electrode. <sup>b</sup> From ref 4. <sup>c</sup> From ref 13. <sup>d</sup> From ref 58. <sup>e</sup> From ref 59.

**TABLE 2: Free Energy  $\Delta G_{\text{ET}}$  of the Electron Transfer Process in the POPOP–Donor Molecule Systems**

electron-donor molecule	$E_{1/2}^{\text{ox}}(\text{D/D}^+) - E_{1/2}^{\text{red}}(\text{A}^{\cdot-}/\text{A})$ [eV]	$a$ [Å]	$\epsilon_{\text{P.G.}}$	$e^2/4\pi\epsilon_0 a$ [eV]	$\Delta G_{\text{ET}}$ [eV]
DEA	2.53	7	32	0.06	−0.80
TMB	2.89	7	32	0.06	−0.44
KI	2.67	7	32	0.06	−0.66

Carbon tetrachloride is well-known as an electron-acceptor quencher for fluorescent aromatic amines<sup>14–16</sup> and aromatic hydrocarbons.<sup>18–22</sup> However, carbon tetrachloride does not quench the fluorescence of POPOP in propylene glycol. Moreover, fluorescence emission of POPOP is observed even in pure carbon tetrachloride as the solvent. This is understandable based on the fact that both carbon tetrachloride and POPOP act as electron acceptors and the electron transfer mechanism of quenching is not effective in this system. Nevertheless, the fluorescence emission of POPOP is efficiently quenched by carbon tetrabromide<sup>50</sup> and less efficiently quenched by methyl iodide and bromoform, which can also act as electron acceptors. The electron transfer mechanism cannot be used for explanation of the quenching ability of methyl iodide. The reduction potential of methyl iodide is much lower than the reduction potential of carbon tetrachloride (see Table 1); therefore, the electron transfer quenching of the POPOP fluorescence by methyl iodide is even less probable. The mechanism of quenching by the less efficient quenchers methyl iodide and bromoform can be due to the heavy atom effect on the singlet state of POPOP. The high efficiency of quenching observed for carbon tetrabromide<sup>50</sup> can be explained by the heavy atom effect and its relatively high value of the reduction potential (Table 1), which can increase the probability of electron transfer from singlet excited POPOP molecules to the quencher. The mechanism of quenching due to the external heavy atom effect can be explained by the exciplex or encounter complex formation in the singlet state of POPOP. The heavy atoms increase the intersystem crossing process (ISC) to form a triplet exciplex or encounter complex that dissociates according to the scheme



In this process the short-lived intermediate states are not detectable. This scheme is generally accepted<sup>23–27,61</sup> and indicates that external heavy atom fluorescence quenching occurs when the heavy atom is in the environment of the fluorescing molecule causing spin–orbit coupling. This quenching is short-range, requiring close contact between the fluorophore and heavy atom quencher.

We used frequency-domain time-resolved and steady-state fluorescence measurements of the POPOP intensity decays to

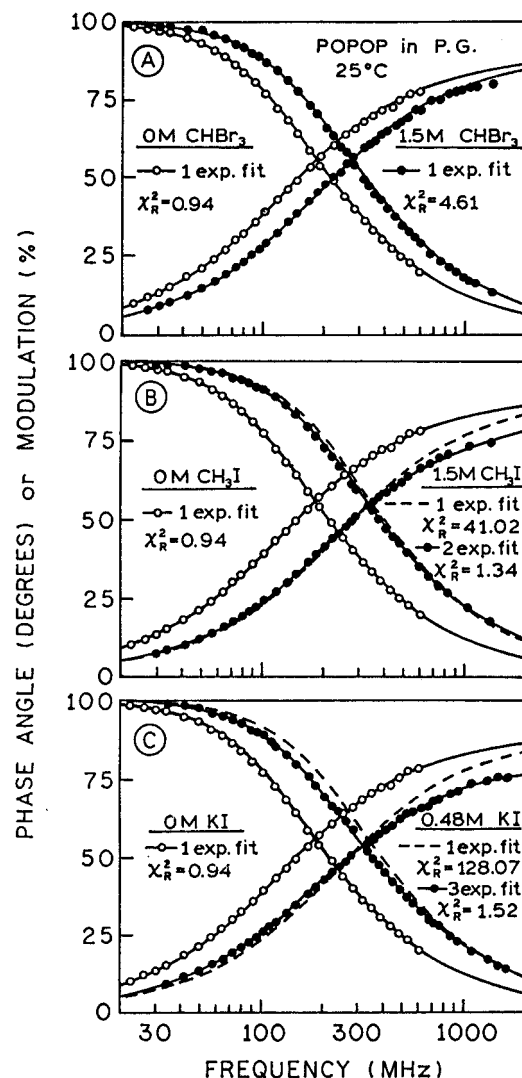


**Figure 3.** Frequency response of the POPOP intensity decay in propylene glycol at 25 °C. The open circles (○) and solid lines represent the data and best single-exponential fits in the absence of quenchers. The closed circles (●) and solid lines represent the data and best single-exponential fit with 1.5 M CHBr<sub>3</sub> (A), two-exponential fit with 1.5 M CH<sub>3</sub>I (B), and three-exponential fit with 0.48 M KI (C). The dashed lines show the best single-exponential fits to data.

investigate the nature of the interactions with several quenchers, which in order of increasing quenching ability are bromoform, methyl iodide, potassium iodide, TMB, and DEA. We also used the RBC<sup>53–55</sup> and DDQ<sup>21,50–52</sup> quenching models, which provide distinct intensity decays.

Frequency responses of the POPOP intensity decays in propylene glycol at 25 °C in the absence and presence of quenching are shown in Figures 3 and 4. It can be seen that in the absence of quenching the fluorescence intensity decay of POPOP is a single exponential and experimental data points are fitted with a single decay time  $\tau = 1.27$  ns ( $\chi^2_R = 0.94$ ). In the presence of quenching the single-exponential fits are not acceptable to account for the experimental data, as can be judged by the large values of the goodness-of-fit parameter  $\chi^2_R$  (see also Tables 3 and 4). The complex decays of the fluorescence intensity of POPOP in the presence of quenching are the result of the transient effects<sup>21,44–46</sup> due to diffusion and short-range through-space interactions between POPOP and quencher molecules. Only for bromoform (1.5 M) does the single-exponential model with  $\tau = 0.858$  ns have a reasonably low value of  $\chi^2_R = 4.61$ . For methyl iodide (1.5 M)  $\chi^2_R = 41.02$ , and a two-decay time fit with  $\tau_1 = 0.723$  ns ( $\alpha_1 = 0.80$ ) and  $\tau_2$

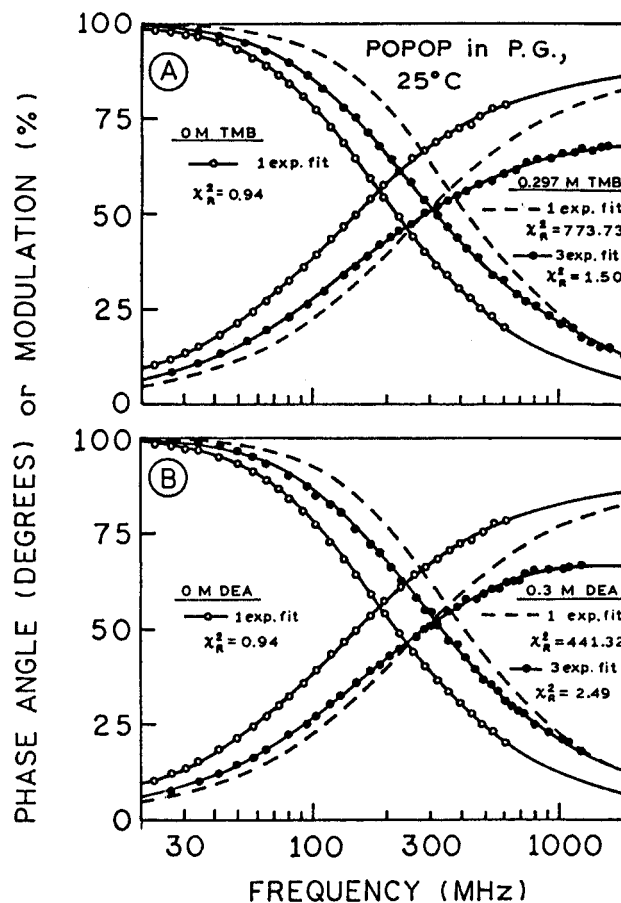


**Figure 4.** Frequency response of the POPOP intensity decay in propylene glycol at 25 °C. The open circles (○) and solid lines represent the data and best single-exponential fits in the absence of quenchers. The closed circles (●) and solid lines represent the data and best three-exponential fits with 0.297 M TMB (A) and 0.3 M DEA (B). The dashed lines show the best single-exponential fits to data.

**TABLE 3: Multiexponential Analysis of POPOP Fluorescence Intensity Decays Quenched by Bromoform, Methyl Iodide, and Potassium Iodide in Propylene Glycol at 25 °C**

quencher	$C_q^0$ [M]	$\tau_i$ [ns]	$\bar{\tau}$ [ns]	$\alpha_i$	$f_i$	$\chi^2_R$		
						1 exp	2 exp	3 exp
bromoform	0	1.27	1.27	1.0	1.0	0.94		
	0.5	1.122	1.117	0.961	0.995	4.29	1.98	
		0.144		0.039	0.005			
methyl iodide	1.5	0.870	0.868	0.844	0.998	4.61	1.76	
		0.010		0.156	0.002			
	0.5	1.054	1.021	0.860	0.956	20.62	1.32	
potassium iodide		0.295		0.140	0.044			
	1.5	0.723	0.702	0.800	0.967	41.02	1.34	
		0.098		0.200	0.033			
	0.10	1.166	1.143	0.881	0.975	21.29	0.74	
		0.223		0.119	0.025			
	0.30	1.029	0.934	0.612	0.824	68.65	2.94	1.93
		0.528		0.233	0.161			
		0.071		0.155	0.015			
	0.48	0.842	0.776	0.371	0.887	128.07	2.83	1.52
		0.282		0.127	0.102			
		0.008		0.502	0.011			

$= 0.098$  ns ( $\alpha_2 = 0.20$ ) is needed to fit the data ( $\chi^2_R = 1.34$ ). For potassium iodide (0.48 M)  $\chi^2_R = 128.07$ , and a three-decay time fit with  $\tau_1 = 0.842$  ns ( $\alpha_1 = 0.371$ ),  $\tau_2 = 0.282$  ns ( $\alpha_2 = 0.127$ ), and  $\tau_3 = 0.008$  ns ( $\alpha_3 = 0.502$ ) is needed to fit satisfactorily the data with  $\chi^2_R = 1.52$ . This effect is even more pronounced for TMB (0.297 M) and DEA (0.3 M), for which monoexponential intensity decay fits yield  $\chi^2_R = 773.73$  and

**TABLE 4: Multiexponential Analysis of POPOP Fluorescence Intensity Decays Quenched by 1,2,4-Trimethoxybenzene and *N,N*-Diethylaniline in Propylene Glycol at 25 °C**

quencher	$C_q^0$ [M]	$\tau_i$ [ns]	$\bar{\tau}$ [ns]	$\alpha_i$	$f_i$	$\chi_R^2$		
						1 exp	2 exp	3 exp
TMB	0.10	1.138	1.106	0.824	0.966	57.39	2.21	
		0.185		0.176	0.034			
		0.549		0.268	0.220			
	0.20	0.170	0.987	0.422	0.737	327.16	5.59	2.68
		0.094		0.310	0.043			
		0.275		0.216	0.154			
DEA	0.1	1.027	0.879	0.306	0.814	773.73	9.61	1.50
		0.026		0.478	0.032			
		0.138		0.173	0.026			
	0.2	1.118	1.093	0.821	0.974	55.34	1.33	
		1.092	0.941	0.049	0.760	190.25	5.33	1.87
		0.515		0.030	0.215			
	0.3	0.002		0.921	0.025			
		1.028	0.844	0.279	0.709	441.32	7.68	2.49
		0.460		0.216	0.246			
		0.036		0.505	0.045			

$\chi_R^2 = 441.32$ , respectively (Figure 4). Both quenchers require three-exponential intensity decay fits to satisfactorily fit the data. The multiexponential analyses yield for TMB  $\tau_1 = 1.027$  ns ( $\alpha_1 = 0.306$ ),  $\tau_2 = 0.275$  ns ( $\alpha_2 = 0.216$ ), and  $\tau_3 = 0.026$  ns ( $\alpha_3 = 0.478$ ) with  $\chi_R^2 = 1.50$ , and for DEA  $\tau_1 = 1.028$  ns ( $\alpha_1 = 0.279$ ),  $\tau_2 = 0.460$  ns ( $\alpha_2 = 0.216$ ), and  $\tau_3 = 0.036$  ns ( $\alpha_3 = 0.505$ ) with  $\chi_R^2 = 2.49$ .

As shown in Figures 3 and 4, the intensity decays of POPOP become heterogeneous in the presence of quenching. This effect is progressively larger for more efficient quenching going from bromoform and methyl iodide, to potassium iodide, to TMB and DEA. As the concentration of quencher increases, the fluorescence intensity decays of POPOP also become increasingly heterogeneous. This results in progressive shifting of the frequency response to higher frequencies, corresponding to a decrease in mean decay time ( $\bar{\tau}$ ) from 1.27 ns to 0.868 and 0.702 ns for bromoform and methyl iodide, co-respectively, to 0.776 ns for potassium iodide, to 0.879 ns for TMB, and to 0.844 ns for DEA at the highest quencher concentration used (see Tables 3 and 4).

The frequency-domain intensity decays and steady-state intensities of POPOP in propylene glycol for the different quencher concentrations were analyzed globally using the RBC and DDQ models. The intensity decay data of POPOP in the presence of different quenchers are presented in Figures 5 and 6. The variable global parameters are  $D$  and  $\kappa$  for the RBC model and  $D$ ,  $k_a$ , and  $r_e$  for the DDQ model. For both models during the analysis the estimated values of  $a$  were kept as the same fixed value. For the RBC analyses  $D$  and  $\kappa$  (or exclusively  $a$ ) were floating parameters. We often observed during the least-squares analysis that the value of  $\kappa$  tended toward infinity. When  $\kappa$  reached a value of  $10^{10}$  cm/s during the least-squares minimization, it was equivalent to  $\infty$  for the RBC model. On the other hand, during the DDQ analyses  $D$ ,  $k_a$ , and  $r_e$  were kept as floating parameters. For both types of analyses RBC and DDQ we combined the frequency-domain and steady-state decay data. Previously we discovered that in the case of more efficient quenchers, such as DEA,<sup>52,62</sup> the combined DDQ analysis of both types of data allows for simultaneous evaluation of the parameters  $k_a$  and  $r_e$ , which are highly correlated using just the frequency-domain data.

The results of the global RBC and DDQ analyses are shown in Tables 5 and 6, assuming different fixed values of the distance of the closest approach  $a$  equal to 5, 6, and 7 Å, for potassium iodide; 7 Å for bromoform and methyl iodide; and 7, 8, and 9

Å for TMB and DEA. The distance  $a$  equal to 7 Å was chosen on the basis of the previously evaluated  $a$  value for the POPOP–carbon tetrabromide system<sup>50</sup> and was used in analyses for all quenchers. Other values allowed a more extended investigation of the applications of the models to POPOP–quencher interactions.

In Figures 5 and 6 the solid lines represent the best global fits obtained using the DDQ model and the dashed lines represent the fits obtained using the RBC model. As can be seen in Figure 5, both models account for the frequency-domain intensity decays and steady-state quantum yield data for POPOP quenched by bromoform and methyl iodide using  $a = 7$  Å. This is reflected by the good visual agreement between the measured and calculated data and by the low  $\chi_R^2$  values presented in Table 5. However, for POPOP quenched by potassium iodide (see Figure 5C) the RBC model using  $a = 7$  Å is less precisely consistent with the frequency-domain and steady-state data ( $\chi_R^2 = 6.84$ ). This model requires a larger distance of  $a = 11.6$  Å to precisely fit the quenching data. Moreover, the RBC model cannot account at all for the intensity decays and steady-state data of POPOP quenched by TMB and DEA. This is emphasized by the lack of agreement between the calculated and measured frequency-domain and steady-state data values (see Figure 6) and by the highly elevated  $\chi_R^2$  even with the largest and nonrealistic values of  $a$  equal to 36.8 Å for TMB and 81.5 Å for DEA. In contrast to the RBC model, the DDQ model is consistent with the measured frequency domain and steady-state data for POPOP quenched by potassium iodide, TMB, and DEA. In this case for each quencher there is excellent agreement between the data and the best-fit curves (see Figures 5C and 6) with the low  $\chi_R^2$  values (see Tables 5 and 6).

Examination of the RBC analysis in Figures 5 and 6 reveals that in the case of TMB and DEA the RBC model cannot provide the smaller phase angles at high modulation frequency required by the data. Smaller phase angles are associated with shorter lived components in the intensity decay. The effect of the distance-dependent quenching rate is to create a short-lived component in the initial part of the decay. This is clearly seen in Figures 7 and 8, which show the time-dependent intensity decays as recovered from the frequency-domain data. For bromoform and methyl iodide (Figure 7) the short-lived components make only a small contribution to the intensity decay. The short-lived component near 20 ps appears larger for potassium iodide (Figure 7C) and makes a still larger contribution in the POPOP intensity decay in the presence of TMB and DEA (Figure 8). An advantage of the DDQ model is its ability to explain the upward curvature in the Stern–Volmer plots (Figures 5 and 6). Within this model the experimental and calculated quantum yields are in agreement for the same parameter values as for the frequency-domain data.

In the discussion of the parameter values recovered from the frequency-domain and steady-state intensity data using the DDQ and RBC analysis it is of interest to compare the diffusion coefficients obtained from the data analysis with those calculated from diffusion theory. The diffusion coefficients of POPOP, DEA, TMB, KI, CH<sub>3</sub>I, and CHBr<sub>3</sub> in propylene glycol at 25 °C were calculated on the basis of the Stokes–Einstein equation:

$$D = k_B T / 6\pi R \eta \quad (3)$$

where  $k_B$  is the Boltzman constant,  $T$  is the temperature in K,  $\eta$  is the viscosity of propylene glycol (36.4 cP at 25 °C), and  $R$  is the radius of the molecule. Considering the van der Waals radii of the molecules, using molecular models we estimated  $R$  as an average radius from the relation  $R = (3V/4\pi)^{1/3}$ .<sup>63</sup>  $V$  is the molecular volume expressed by  $(4/3)\pi r_x r_y r_z$ , where  $r_x$ ,  $r_y$ ,

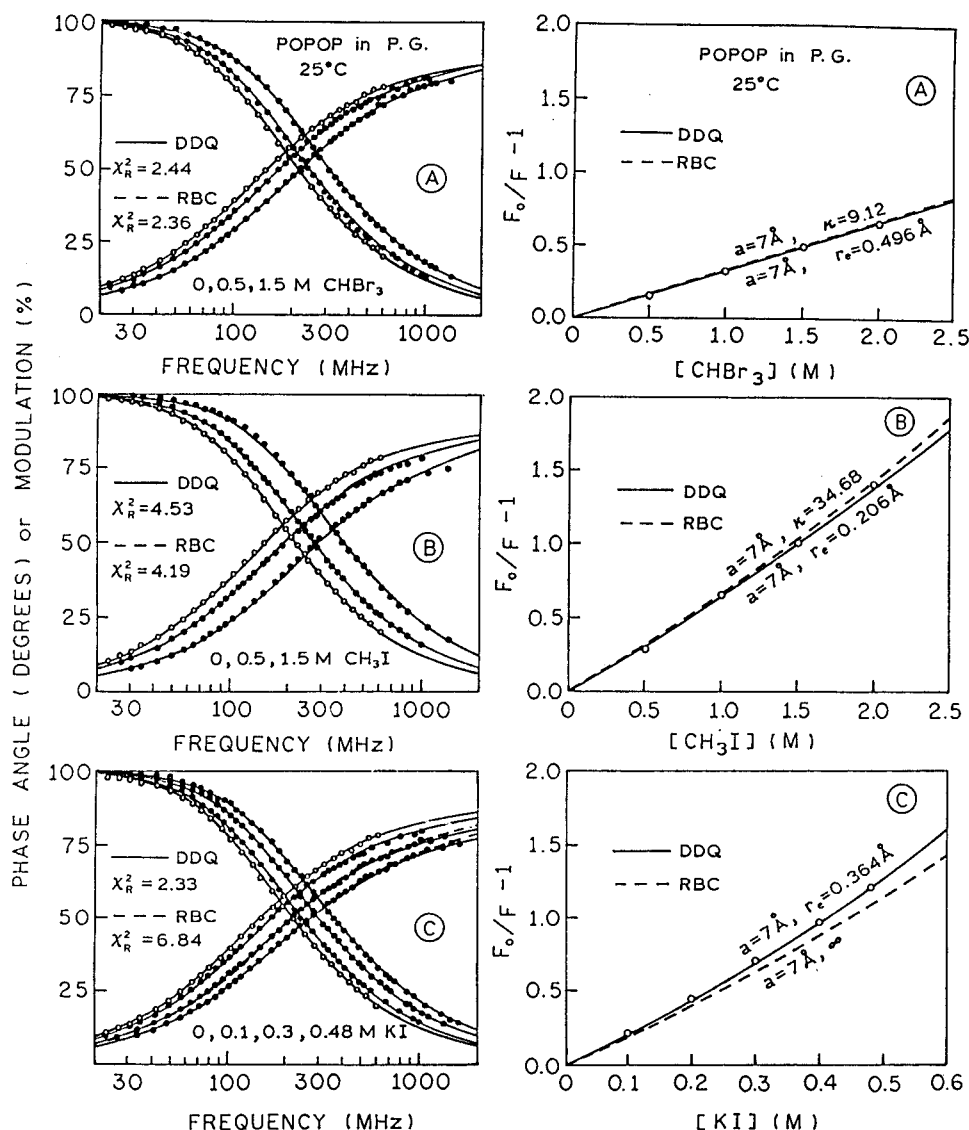


**Figure 5.** (Left) Frequency-domain intensity decays of POPOP in propylene glycol at 25 °C in the presence of increasing (left to right) concentrations of  $\text{CHBr}_3$  (0, 0.5, and 1.5 M) (A),  $\text{CH}_3\text{I}$  (0, 0.5, and 1.5 M) (B), and  $\text{KI}$  (0, 0.1, 0.3, and 0.48 M) (C). The solid lines show the best fit to the DDQ model using for  $\text{CHBr}_3$   $a = 7 \text{ \AA}$  and  $r_e = 0.436 \text{ \AA}$ , for  $\text{CH}_3\text{I}$   $a = 7 \text{ \AA}$  and  $r_e = 0.206 \text{ \AA}$ , and for  $\text{KI}$   $a = 7 \text{ \AA}$  and  $r_e = 0.364 \text{ \AA}$ , respectively. The dashed lines (A, B, and C) show the best fit to the RBC model using  $a = 7 \text{ \AA}$ . (Right) Stern–Volmer plots for POPOP in propylene glycol at 25 °C quenched by  $\text{CHBr}_3$  (A),  $\text{CH}_3\text{I}$  (B), and  $\text{KI}$  (C) (open circles). The solid lines represent the calculated values of  $(F_0/F) - 1$  using parameter values from the DDQ model for  $a = 7 \text{ \AA}$ . The dashed lines represent the RBC model using also  $a = 7 \text{ \AA}$  (see Table 5).

and  $z$  are the van der Waals radii of the molecule in the  $x$ ,  $y$ , and  $z$  directions. The van der Waals radii and the diffusion coefficients of the fluorophore and quencher molecules are summarized in Table 7.

The diffusion coefficients recovered from the intensity decay data for  $\text{CHBr}_3$ ,  $\text{CH}_3\text{I}$ , and  $\text{KI}$  using DDQ and RBC models are in good agreement with those values predicted from the diffusion theory (see Tables 7 and 5). This agreement of the  $D$  values is observed for the weak quenching interactions. However, in the case of the strong quenching effect, for TMB and for DEA the RBC model provides values of  $D$  that for a reasonable encounter distance are larger than the expected values (see Tables 7 and 6). This might be due to the effect of compensation for the initial drop of the intensity decays, which introduce some additional quenching.<sup>62</sup> In contrast to the RBC the DDQ model for TMB and for DEA results in values of  $D$  that are several-fold smaller than the expected values calculated from the Stokes–Einstein equation. This effect can be explained by the fluorophore–solvent or quencher–solvent interactions, which slow diffusion and/or increase the size of the diffusing species.

Collisional quenching of POPOP by  $\text{CHBr}_3$  and  $\text{CH}_3\text{I}$  appears to be a heavy atom effect characterized by comparatively weak intermolecular interactions that occur at short distance. This distance can be estimated as the sum of the average van der Waals radii of fluorophore and quencher molecules (see Table 7), which may be increased by the solvent–cage effect, giving reasonable value of  $a = 7 \text{ \AA}$ . From the RBC model the quenching is characterized by the low value of  $\kappa$  equal to 9.12 and 34.67 cm/s for  $\text{CHBr}_3$  and  $\text{CH}_3\text{I}$ , respectively. Moreover DDQ analysis yields bimolecular rate constants  $k_a$  on the order of  $10^{10}$ , with a characteristic distance  $r_e \leq 0.5 \text{ \AA}$ . For the more efficient quenching by  $\text{KI}$  the DDQ analysis provides the bimolecular rate constant on the order of  $10^{11}$  with  $r_e$  values ranging from 0.625 at  $a = 5 \text{ \AA}$  to 0.364 at  $a = 7 \text{ \AA}$ . For the RBC analysis  $\kappa \rightarrow \infty$  and  $a$  increases from 7 to 11.6 Å for an acceptable value of  $\chi_R^2 = 2.89$ . The distance of  $a = 11.6 \text{ \AA}$  for  $\text{KI}$  is still a realistic distance, indicating that not only electron exchange but also electron transfer interactions are involved in the mechanisms of quenching. For POPOP quenched by TMB and DEA the reasonable distance of  $a$  is also estimated at 7 Å

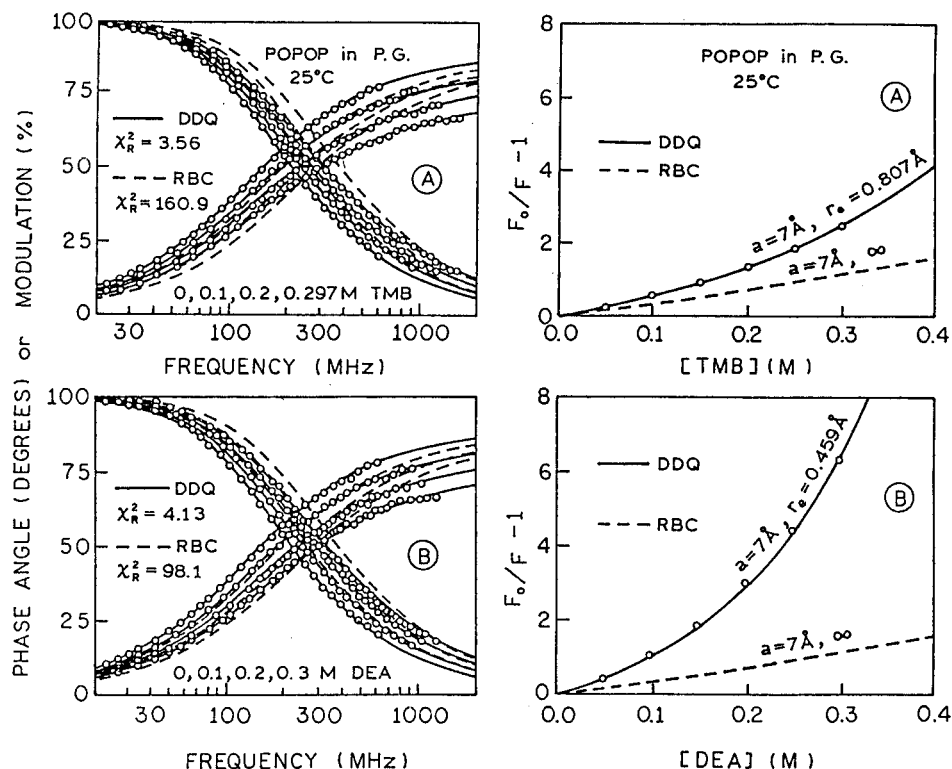


**Figure 6.** (Left) Frequency-domain intensity decays of POPOP in propylene glycol at 25 °C in the presence of increasing (left to right) concentrations of TMB (0, 0.1, 0.2, and 0.297 M) (A) and DEA (0, 0.1, 0.2, and 0.3 M) (B). The solid lines show the best fit to the DDQ model using for TMB  $a = 7$  Å and  $r_e = 0.807$  Å and for DEA  $a = 7$  Å and  $r_e = 0.459$  Å. The dashed lines (A and B) show the best fit to the RBC model using  $a = 7$  Å. (Right) Stern–Volmer plots for POPOP in propylene glycol at 25 °C quenched by TMB (A) and DEA (B) (open circles). The solid lines represent the calculated values of  $(F_0/F) - 1$  using parameter values from the DDQ model for  $a = 7$  Å. The dashed lines represent the RBC model using also  $a = 7$  Å (see Table 6).

**TABLE 5: Global Analysis of POPOP Quenching by Bromoform, Methyl Iodide, and Potassium Iodide in Propylene Glycol at 25 °C ( $\tau_0 = 1.27$  ns)**

quencher	$a$ [Å]	DDQ analysis				RBC analysis		
		$r_e$ [Å]	$D$ [ $10^{-7}$ cm <sup>2</sup> /s]	$k_a$ [ $10^{10}$ 1/s]	$\chi_R^2$	$\kappa$ [cm/s]	$D$ [ $10^{-7}$ cm <sup>2</sup> /s]	$\chi_R^2$
CHBr <sub>3</sub> <sup>a</sup>	$\langle 7 \rangle^c$	0.496 (0.454–0.575) <sup>d</sup>	4.14 (3.83–5.04)	0.14 (0.12–0.16)	2.44	9.12 (8.78–9.46)	4.51 (3.81–5.34)	2.36
CH <sub>3</sub> I <sup>a</sup>	$\langle 7 \rangle$	0.206 (0.198–0.35)	2.91 (2.62–3.22)	1.14 (0.59–1.25)	4.53	34.68 (32.43–36.22)	2.94 (2.77–3.11)	4.19
KI <sup>b</sup>	$\langle 5 \rangle$	0.625 (0.599–0.645)	7.96 (7.63–8.26)	10.8 (9.08–13.1)	2.29	$\langle \infty \rangle^e$	18.3 (18.1–18.6)	15.38
	$\langle 6 \rangle$	0.488 (0.464–0.505)	7.06 (6.80–7.31)	10.4 (8.72–12.8)	2.30	$\langle \infty \rangle$	12.6 (12.5–12.7)	10.21
	$\langle 7 \rangle$	0.364 (0.342–0.378)	5.96 (5.73–6.12)	11.2 (9.33–14.0)	2.33	$\langle \infty \rangle$	8.81 (8.74–8.88)	6.84
	11.6 (11.0–12.1)					$\langle \infty \rangle$	2.08 (1.77–2.43)	2.89

<sup>a</sup> The concentration of CHBr<sub>3</sub> and CH<sub>3</sub>I ( $C_Q$ ) was 0, 0.5, and 1.5 M. <sup>b</sup> The concentration of KI ( $C_Q$ ) was 0, 0.1, 0.3, and 0.48 M. <sup>c</sup> The angular brackets  $\langle \rangle$  indicate the parameter was held fixed at the indicated value. <sup>d</sup> The numbers in parentheses represent the 67% confidence intervals obtained from the least-squares analysis. <sup>e</sup> In calculations  $\kappa = \infty$  has been represented by setting  $\kappa = 10^{10}$  cm/s.

on the basis of the van der Waals radii of the molecules. Using the DDQ model, the experimental data can be precisely fitted with  $a = 7$  Å and recovered values of  $r_e = 0.807$  Å,  $D = 4.7 \times 10^{-8}$  cm<sup>2</sup>/s, and  $k_a = 8.34 \times 10^{11}$  s<sup>-1</sup> for TMB, and  $r_e = 0.459$  Å,  $D = 1.43 \times 10^{-7}$  cm<sup>2</sup>/s, and  $k_a = 4.57 \times 10^{15}$  s<sup>-1</sup> for DEA (see Table 6). In both cases the quenching can occur also at larger distances. These values appear to be consistent with the mechanism of quenching due to electron transfer from the fluorophore to the quencher molecules. The bimolecular rate constant  $k_a$  for TMB is approximately 3 orders of magnitude lower than the  $k_a$  value for DEA. Such a decrease in the  $k_a$  value can be correlated with the change in free energy  $\Delta G_{ET}$ .  $\Delta G_{ET}$  is less negative for TMB (−0.44 eV) than for DEA (−0.80 eV). For KI with  $\Delta G_{ET} = -0.66$  eV, the value of  $k_a$  equal to  $1.12 \times 10^{11}$  s<sup>-1</sup> does not correlate with the change in

free energy  $\Delta G_{ET}$  presented in Table 2. The lower than expected value of  $k_a$  indicates that for KI the bimolecular rate constant of quenching versus free energy is in that part of the function that is named “Marcus inverted region”.<sup>64</sup> This is possibly due to the effect of dielectric saturation of the solvent in the field of iodide ions.

The characteristic distance of the fluorophore–quencher interaction  $r_e$  is correlated with the encounter distance  $a$  and typically decreases<sup>62</sup> when  $a$  is changed to longer values. This is shown for KI, TMB, and DEA in Tables 5 and 6. Moreover, the  $r_e$  value somehow characterizes the quencher–solvent interactions. Elevated values of  $r_e$  are observed for KI and TMB where the ionic field of iodide and the potential of hydrogen-bonding interactions with methoxy groups of TMB are expected to affect the solvent molecules.



**TABLE 6: Global Analysis of POPOP Quenching by 1,2,4-Trimethoxybenzene and *N,N*-Diethylaniline in Propylene Glycol at 25 °C ( $\tau_0 = 1.27$  ns)**

quencher	$a$ [Å]	DDQ analysis				RBC analysis		
		$r_e$ [Å]	$D$ [ $10^{-7}$ cm <sup>2</sup> /s]	$k_a$ [ $10^{13}$ 1/s]	$\chi_R^2$	$\kappa$ [cm/s]	$D$ [ $10^{-7}$ cm <sup>2</sup> /s]	$\chi_R^2$
TMB <sup>a</sup>	$\langle 7 \rangle^c$	0.807	0.47	0.0084	3.56	$\langle \infty \rangle^e$	20.2	160.9
		(0.792–0.822) <sup>d</sup>	(0.39–0.56)	(0.0067–0.0099)			(19.4–21.0)	
	$\langle 8 \rangle$	0.746	0.55	0.0060	3.43	$\langle \infty \rangle$	15.0	144.8
		(0.729–0.759)	(0.47–0.64)	(0.0051–0.0072)			(14.5–15.6)	
	$\langle 9 \rangle$	0.679	0.60	0.0048	3.31	$\langle \infty \rangle$	11.3	131.5
DEA <sup>b</sup>		(0.667–0.692)	(0.53–0.67)	(0.0039–0.0055)			(10.9–11.7)	
	36.8					$\langle \infty \rangle$	0.063	98.9
	(23.7–40.5)						(0.049–0.355)	
	$\langle 7 \rangle$	0.459	1.43	457	4.13	$\langle \infty \rangle$	19.2	98.1
		(0.450–0.466)	(1.34–1.52)	(313–636)			(18.6–19.7)	
	$\langle 8 \rangle$	0.437	1.35	175	4.13	$\langle \infty \rangle$	14.2	87.5
		(0.429–0.444)	(1.28–1.44)	(130–238)			(13.8–14.6)	
	$\langle 9 \rangle$	0.410	1.26	96	4.11	$\langle \infty \rangle$	10.6	79.0
		(0.401–0.417)	(1.18–1.34)	(65–135)			(10.4–10.9)	
	81.5					$\langle \infty \rangle$	0.003	44.5
	(75.0–88.8)						(0.002–0.005)	

<sup>a</sup> The concentration of TMB ( $C_Q$ ) was 0, 0.1, 0.2, and 0.297 M. <sup>b</sup> The concentration of DEA ( $C_Q$ ) was 0, 0.1, 0.2, and 0.3 M. <sup>c</sup> The angular brackets  $\langle \rangle$  indicate the parameter was held fixed at the indicated value. <sup>d</sup> The numbers in parentheses represent the 67% confidence intervals obtained from the least-squares analysis. <sup>e</sup> In calculations  $\kappa = \infty$  has been represented by setting  $\kappa = 10^{10}$  cm/s.

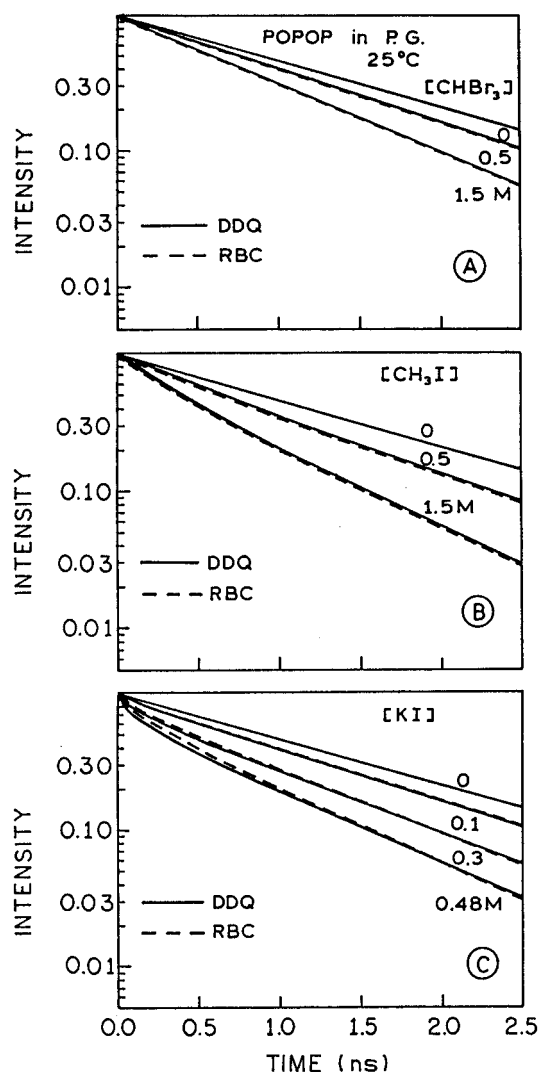


**Figure 7.** Reconstructed time-dependent intensity decays of POPOP in propylene glycol at 25 °C quenched by CHBr<sub>3</sub> (0, 0.5, and 1.5 M) (A), CH<sub>3</sub>I (0, 0.5, and 1.5 M) (B), and KI (0, 0.1, 0.3, and 0.48 M) (C), for the best-fit RBC (---) and DDQ (—) parameters using  $a = 7$  Å.

Figures 5 and 6 and summarized data of global analyses in Tables 5 and 6 clearly show that the efficiency of quenching of

**TABLE 7: The van der Waals Radii of the Fluorophore and Quencher Molecules and Their Diffusion Coefficients in Propylene Glycol at 25 °C**

molecule	$r_x$ [Å]	$r_y$ [Å]	$r_z$ [Å]	$R$ [Å]	$D^c$ [ $10^{-7}$ cm <sup>2</sup> /s]	$D_F + D_Q$ [ $10^{-7}$ cm <sup>2</sup> /s]	DDQ $D^d$ [ $10^{-7}$ cm <sup>2</sup> /s]	RBC $D^e$ [ $10^{-7}$ cm <sup>2</sup> /s]
POPOP	2.0	2.2	6.5	3.3 <sup>a</sup>	1.82			
DEA	1.3	2.5	4.0	2.35 <sup>b</sup>	2.55	4.37	1.43	19.2
TMB	1.0	3.3	4.6	2.48	2.42	4.24	0.47	20.2
KI	1.5	1.5	2.5	1.78	3.37	5.19	5.96	8.81
CH <sub>3</sub> I	1.5	1.5	2.3	1.73	3.47	5.29	2.91	2.94
CHBr <sub>3</sub>	1.5	2.9	2.9	2.33	2.58	4.40	4.14	4.51

<sup>a</sup> From ref 50. <sup>b</sup> From ref 52. <sup>c</sup> Calculated values of  $D$  using Stokes–Einstein equation. <sup>d</sup> Recovered values of  $D$  from the DDQ analysis (Tables 5 and 6). <sup>e</sup> Recovered values of  $D$  from the RBC analysis (Tables 5 and 6).

POPOP increases in the order bromoform, methyl iodide, potassium iodide, TMB, and DEA. This is emphasized by the apparent bimolecular quenching rate, which increases following the order of quencher molecules. Weak quenching effects of bromoform and methyl iodide are due to the heavy atom spin–orbit interactions with POPOP molecule and are reflected by  $k_a$  values equal to  $0.14 \times 10^{10}$  and  $1.14 \times 10^{10}$  s<sup>−1</sup>, respectively. On the other hand, the strong quenching effect observed for TMB and DEA is characterized by the quenching rates being  $8.43 \times 10^{11}$  and  $4.57 \times 10^{15}$  s<sup>−1</sup>, respectively. The significant difference between  $k_a$  values obtained for TMB and DEA can be explained by the less negative value of  $\Delta G_{ET}$  for TMB than for DEA (see Table 4) and also by the solvent–TMB interactions, due to the methoxy groups in the molecule, which slow diffusion of the quencher 2- to 3-fold as compared to the same effect for DEA molecule. The quenching rate for potassium iodide is equal to  $11.2 \times 10^{10}$  s<sup>−1</sup> and seems to reflect the dual character in the quenching mechanism, which involves the electron transfer interactions and the heavy atom effect.

In summary, the results described above illustrate that collisional quenching of fluorescence can result in complex intensity decays. Depending upon the nature of the fluorophore–quencher pair, the intensity decays may or may not be fit by the RBC model. A good fit with the RBC model does not indicate that the quenching rate constant is independent of distance, but only that the dependence may not be evident in the time-resolved data. Careful analysis of the steady-state and

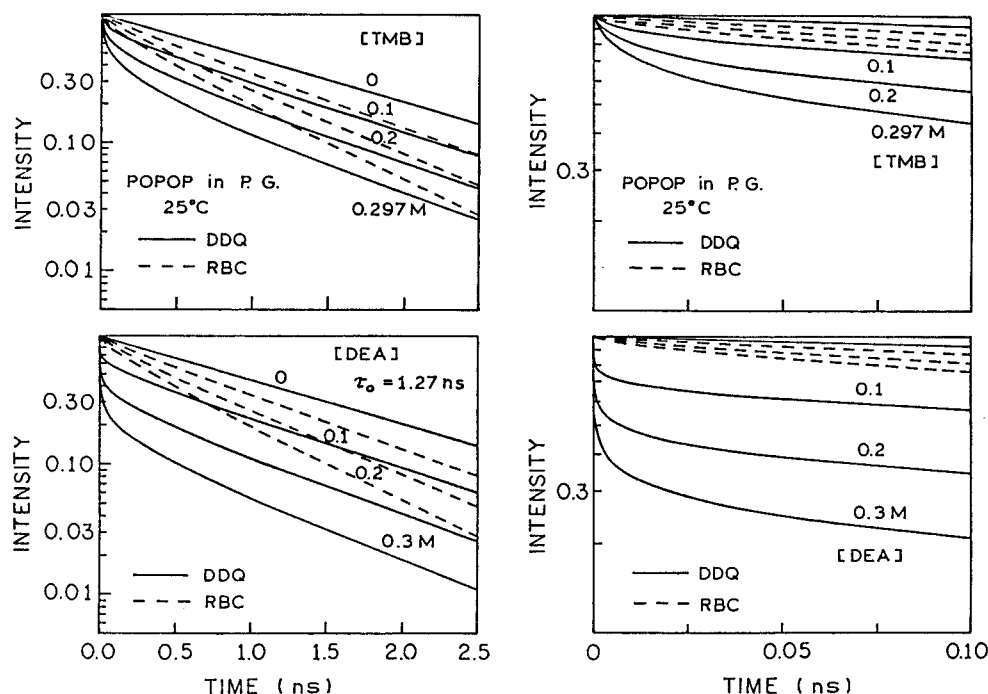


**Figure 8.** Reconstructed time-dependent intensity decays of POPOP in propylene glycol at 25 °C quenched by TMB (0, 0.1, 0.2, and 0.297 M) (upper panels) and DEA (0, 0.1, 0.2, and 0.3 M) (lower panels), for the best-fit RBC (---) and DDQ (—) parameters using  $a = 7 \text{ \AA}$ .

time-resolved data can provide some insight into the mechanism of quenching.

The existence of distance-dependent quenching also implies the presence of a through-space interaction. In the case of long decay times this interaction can lead to quenching over considerable distances.<sup>36</sup> This possibility, and the presence of complex intensity decays even for single-exponential fluorophores, needs to be considered in the analysis of quenching data of proteins and biopolymers.

**Acknowledgment.** This work was supported by a grant from the National Institutes of Health (GM-39617) with support for instrumentation from NSF DIR-8710401, NIH RR-07510, and NIH RR-08119.

### Appendix: Theory

The fluorescence intensity decay of a fluorophore with a single exponential is given by

$$I(t) = I_0 \exp(-t/\tau_0) \quad (4)$$

where  $\tau_0$  is the decay time. For a multiexponential intensity decay

$$I(t) = I_0 \sum_i \alpha_i \exp(-t/\tau_i) \quad (5)$$

where  $\alpha_i$  are the amplitudes associated with the individual decay times  $\tau_i$ . The amplitudes  $\alpha_i$  are normalized so that  $\sum \alpha_i = 1$ . The fractional contribution of each decay time component to the steady-state intensity is expressed as

$$f_i = \frac{\alpha_i \tau_i}{\sum_j \alpha_j \tau_j} \quad (6)$$

The mean decay time is given by  $\bar{\tau} = \sum f_i \tau_i$ .

The time-dependent intensity decay of the fluorophore in the presence of diffusive quenching is complex and is given by

$$I(t) = I_0 \exp \left[ -\frac{t}{\tau_0} - C_q^0 \int_0^t k(t') dt' \right] \quad (7)$$

where  $\tau_0$  is the fluorophore lifetime in the absence of quenching,  $C_q^0$  is the bulk concentration of the quencher, and  $k(t)$  denotes the averaged time-dependent fluorophore–quencher reaction rate. The rate  $k(t)$  is expressed as

$$k(t) = \frac{4\pi}{C_q^0} \int_a^\infty r^2 k(r) C_q(r,t) dr \quad (8)$$

where  $C_q(r,t)$  is the concentration of the quencher molecules at a distance  $r$  from the excited fluorophore at time instant  $t$ . To simplify the calculations, one introduces the function  $y(r,t) = C_q(r,t)/C_q^0$ . In the presence of diffusion the function  $y(r,t)$  is governed by the diffusion equation. The equation has an additional sink term, which is responsible for the through-space fluorescence quenching,

$$\frac{\partial y(r,t)}{\partial t} = D \nabla^2 y(r,t) - k(r) y(r,t) \quad (9)$$

where  $D = D_F + D_Q$  is the mutual diffusion coefficient of the fluorophore and the quencher with diffusion coefficients  $D_F$  and  $D_Q$ , respectively. For the RBC model through-space fluorescence quenching does not take place, and then the additional sink term  $-k(r) y(r,t)$  in eq 9 disappears. For both quenching models the initial and outer boundary conditions of eq 9 remain the same

$$y(r,t=0) = 1 \quad (10)$$

$$\lim_{r \rightarrow \infty} y(r,t) = 1 \quad (11)$$

The form of the inner boundary condition (at  $r = a$ ) depends on the particular model. For the RBC model we have

$$\left[ \frac{\partial y(r,t)}{\partial r} \right]_{r=a} = \frac{\kappa}{D} y(r=a,t) \quad (12)$$

whereas for DDQ model one assumes the “reflecting” or “specular” boundary condition at  $r = a$ ,

$$\left[ \frac{\partial y(r,t)}{\partial r} \right]_{r=a} = 0 \quad (13)$$

This condition indicates that donor–quencher encounters do not introduce any other deactivation channel apart from that described by the rate  $k(r)$ .

For the RBC model the diffusion equation (9) can be solved analytically yielding<sup>65</sup>

$$\int_0^t k(t') dt' = \frac{4\pi D a k_0}{4\pi D a + k_0} \left\{ t + \frac{k_0}{4\pi D^2 a \alpha^2} \left[ \exp(\alpha^2 D t) \operatorname{erfc}(\alpha \sqrt{D t}) + 2\alpha \frac{\sqrt{D t}}{\sqrt{\pi}} - 1 \right] \right\} \quad (14)$$

where  $k_0 = 4\pi a^2 \kappa$  and  $\alpha = (4\pi D a + k_0)/(4\pi D a^2)$ .

For the DDQ model an exact analytical solution of eq 9 is not possible, and numerical methods are required. In this paper we used the algorithm described previously<sup>66,67</sup> based on the numerical solution of eq 9 in the Laplace space<sup>68</sup> and numerical integration of eq 8.

Using the technique of frequency-domain fluorometry,<sup>47,48</sup> one compares the experimental phase ( $\phi_\omega$ ) and modulation ( $m_\omega$ ) values with those calculated (c) from the model intensity decay  $I(t)$ . At given modulation frequency ( $\omega$ ) these values are given by

$$\phi_{c\omega} = \arctan(N_\omega/D_\omega) \quad (15)$$

$$m_{c\omega} = \frac{1}{J} (N_\omega^2 + D_\omega^2)^{1/2} \quad (16)$$

where

$$N_\omega = \int_0^\infty I(t) \sin(\omega t) dt \quad (17)$$

$$D_\omega = \int_0^\infty I(t) \cos(\omega t) dt \quad (18)$$

$$J = \int_0^\infty I(t) dt \quad (19)$$

The fluorophore quantum yield is another experimental observable, which can also be predicted by the quenching models. In this paper we examined the Stern–Volmer-type quantity  $f$  defined as

$$f = F_0/F - 1 \quad (20)$$

where  $F_0$  and  $F$  are fluorophore quantum yields in the absence and presence of quencher. The ratio  $F/F_0$  expresses the relative quantum yield of the fluorophore and is given by

$$F/F_0 = \int_0^\infty I(t) dt / \int_0^\infty I_0(t) dt \quad (21)$$

where  $I(t)$  is expressed by eq 7 for either the RBC or DDQ models and  $I_0(t)$  is the fluorophore's intensity decay in the absence of quencher expressed by eq 4, for POPOP, which displays a single-exponential decay without quenching.

It is known that resolution of correlated parameters can be improved by global analyses.<sup>69</sup> For analysis of the data we developed a program that allowed global analysis of both the intensity decay and steady-state data. This program was developed because in previous studies<sup>50–52,62</sup> we found that the models (RBC or DDQ) and DDQ parameter values ( $k_a$ ,  $a$ , and  $r_c$ ) were better resolved by ensuring that both the calculated intensity decay and calculated steady-state intensities were consistent with the experimental values. This new program simultaneous fits the frequency-domain intensity decay and steady-state intensities by nonlinear least squares.<sup>70</sup>

The best-fitted parameters and goodness-of-fit are determined by the minimum value of the goodness-of-fit parameter

$$\chi_R^2 = \frac{1}{\nu} \left[ \sum_\omega \left( \frac{\phi_\omega - \omega_{c\omega}}{\delta\phi} \right)^2 + \sum_\omega \left( \frac{m_\omega - m_{c\omega}}{\delta m} \right)^2 + \sum_i \left( \frac{f_i - f_{ci}}{\delta f_i} \right)^2 \right] \quad (22)$$

where  $\nu$  is the number of degrees of freedom and  $\delta\phi$ ,  $\delta m$ , and  $\delta f$  are the experimental uncertainties. For all analyses, the uncertainties  $\delta\phi$  and  $\delta m$  were taken as  $0.2^\circ$  in the phase angle and 0.005 in the modulation ratio, respectively. The uncertainties  $\delta f_i$  were calculated from the relation  $\delta f_i = (F_0/F_i)^2 (\Delta F/F_0)$ . We assume uncertainties of  $\Delta F/F_0 = 0.005$  for POPOP quenched by bromoform, methyl iodide, potassium iodide, TMB, and DEA.

## References and Notes

- (1) Weller, A. *Pure Appl. Chem.* **1968**, 16, 115.
- (2) Weller, A. In *Nobel Symposium 5: Fast Reactions and Primary Processes in Chemical Kinetics*; Claesson, S., Ed.; Almqvist and Wiksell: Stockholm, 1967; p 413.
- (3) Rehm, D.; Weller, A. *Z. Phys. Chem. N. F.* **1970**, 69, 183.
- (4) Rehm, D.; Weller, A. *Ber. Bunsen-Ges. Phys. Chem.* **1969**, 69, 834.
- (5) Rehm, D.; Weller, A. *Isr. J. Chem.* **1970**, 8, 259.
- (6) Taniguchi, Y.; Nishima, Y.; Mataga, N. *Bull. Chem. Soc. Jpn.* **1972**, 45, 764.
- (7) Hino, T.; Akazawa, H.; Masuhara, H.; Mataga, N. *J. Phys. Chem.* **1976**, 80, 33.
- (8) Goldschmidt, C. R.; Potashnik, R.; Ottolenghi, M. *J. Phys. Chem.* **1971**, 75, 1025.
- (9) Miller, J. R.; Peeples, J. A.; Schmitt, M. J.; Closs, G. L. *J. Am. Chem. Soc.* **1982**, 104, 6488.
- (10) Miller, J. R.; Beitz, J. V.; Huddleston, R. K. *J. Am. Chem. Soc.* **1984**, 106, 5057.
- (11) Hui, M.-H.; Ware, W. R. *J. Am. Chem. Soc.* **1976**, 98, 4718.
- (12) Cheung, S. T.; Ware, W. R. *J. Phys. Chem.* **1983**, 87, 466.
- (13) Harman, P. J.; Nott, P. R.; Selinger, B. K. *Aust. J. Chem.* **1977**, 30, 1875.
- (14) Baggott, J. E.; Pilling, M. J. *J. Chem. Soc., Faraday Trans. 1* **1983**, 79, 221.
- (15) Ahmad, A.; Durocher, G. *Photochem. Photobiol.* **1981**, 34, 573.
- (16) Alford, P. C.; Cureton, C. G.; Lampert, R. A.; Phillips, D. *Chem. Phys. Lett.* **1983**, 76, 103.
- (17) Namiki, A.; Nakashima, N.; Yoshihama, K. *J. Chem. Phys.* **1979**, 71, 925.
- (18) Saperstein, D.; Levin, E. *J. Chem. Phys.* **1975**, 62, 3560.
- (19) Leite, M. S. S. C.; Razi Naqvi, K. *Chem. Phys. Lett.* **1969**, 4, 35.
- (20) Behera, P. K.; Mishra, A. K. *J. Photochem. Photobiol. A: Chem.* **1993**, 71, 115.
- (21) Nemzek, T. L.; Ware, W. R. *J. Chem. Phys.* **1975**, 62, 477.
- (22) Encinas, M. V.; Rubio, M. A.; Lissi, E. *Photochem. Photobiol.* **1983**, 37, 125.
- (23) Lessand, G.; Durocher, G. *J. Phys. Chem.* **1978**, 82, 2812.
- (24) Shimizu, Y.; Azumi, T. *J. Phys. Chem.* **1982**, 86, 22.
- (25) Mac, M.; Wirz, J. *Chem. Phys. Lett.* **1993**, 211, 20.
- (26) Najbar, J.; Mac, M. *J. Chem. Soc., Faraday Trans.* **1991**, 87, 1523.
- (27) DeToma, R. P.; Cowan, D. O. *J. Am. Chem. Soc.* **1975**, 97, 3283.
- (28) Green, S. A.; Simpson, D. J.; Zhou, G.; Ho, P. S.; Bhough, N. V. *J. Am. Chem. Soc.* **1990**, 112, 7337.
- (29) Encinas, M. V.; Lissi, E. A.; Alvarez, J. *Photochem. Photobiol.* **1994**, 59, 30.
- (30) Bazhin, N. M.; Gritsan, N. P.; Korolev, V. V.; Camyshin, S. V. *J. Lumin.* **1987**, 37, 87.

- (31) Camyshan, S. V.; Gritsan, N. P.; Korolev, V. V.; Bazhin, N. M. *Chem. Phys.* **1990**, *142*, 59.
- (32) Eftink, M. R. In *Topics in Fluorescence Spectroscopy, Vol. 2: Principles*; Lakowicz, J. R., Ed.; Plenum Press: New York, 1991; p 53.
- (33) Eftink, M. R.; Ghiron, C. A. *Anal. Biochem.* **1981**, *114*, 199.
- (34) Somogyi, B.; Lakos, Z. *J. Photochem. Photobiol. B: Biol.* **1993**, *18*, 3.
- (35) Calhoun, D. B.; Englander, S. W.; Wright, W. W.; Vanderkooi, J. M. *Biochemistry* **1988**, *27*, 8466.
- (36) Vanderkooi, J. M.; Englander, S. W.; Papp, S.; Wright, W. W.; Owen, C. S. *Proc. Natl. Acad. Sci. U.S.A.* **1990**, *87*, 5099.
- (37) Lehrer, S. S. *Biochemistry* **1971**, *10*, 3254.
- (38) Shinitzky, M.; Rivnay, B. *Biochemistry* **1977**, *16*, 982–986.
- (39) Lakowicz, J. R.; Gryczynski, I.; Cherek, H.; Joshi, N. *Eur. Biophys. J.* **1991**, *19*, 125.
- (40) Lakowicz, J. R.; Weber, G. *Biochemistry* **1973**, *12*, 4171.
- (41) Lakowicz, J. R. In *Hemoglobin and Oxygen Binding*; Ho, C., Ed.; Elsevier: New York, 1982; Vol. 1, p 443.
- (42) Stubbs, C. D.; Williams, B. W. In *Topics in Fluorescence Spectroscopy, Vol. 3: Biochemical Applications*; Lakowicz, J. R., Ed.; Plenum Press: New York, 1992; p 231.
- (43) Berlman, I. B. *Handbook of Fluorescence Spectra of Aromatic Molecules*, 2nd ed.; Academic Press, Inc.: New York, 1971.
- (44) Andre, J. C.; Niclaude, M.; Ware, W. R. *Chem. Phys.* **1978**, *28*, 371.
- (45) Lakowicz, J. R.; Joshi, N. B.; Johnson, M. L.; Szmazinski, H.; Gryczynski, I. *J. Biol. Chem.* **1987**, *262*, 10907.
- (46) Lakowicz, J. R.; Johnson, M. L.; Gryczynski, I.; Joshi, N.; Laczko, G. *J. Phys. Chem.* **1987**, *91*, 3277.
- (47) Lakowicz, J. R.; Laczko, G.; Gryczynski, I. *Rev. Sci. Instrum.* **1986**, *57*, 2499.
- (48) Laczko, G. I.; Gryczynski, I.; Gryczynski, Z.; Wicz, W.; Malak, H.; Lakowicz, J. R. *Rev. Sci. Instrum.* **1990**, *61*, 2331.
- (49) Lakowicz, J. R.; Gryczynski, I. *Arabian J. Sci. Eng.* **1990**, *17*, 261.
- (50) Lakowicz, J. R.; Kuśba, J.; Szmazinski, H.; Johnson, M. L.; Gryczynski, I. *Chem. Phys. Lett.* **1993**, *206* (5,6), 455.
- (51) Lakowicz, J. R.; Zelent, B.; Gryczynski, I.; Kuśba, J.; Johnson, M. L. *Photochem. Photobiol.* **1994**, *60*, 205.
- (52) Zelent, B.; Kuśba, J.; Gryczynski, I.; Lakowicz, J. R. *Appl. Spectrosc.* **1995**, *49*, 43.
- (53) Smoluchowski, M. Z. *Phys. Chem.* **1917**, *92*, 129.
- (54) Collins, F. C.; Kimball, G. E. *J. Colloid Sci.* **1949**, *4*, 425.
- (55) Joshi, N.; Johnson, M. L.; Gryczynski, I.; Lakowicz, J. R. *Chem. Phys. Lett.* **1987**, *135*, 200.
- (56) Dexter, D. L. *J. Chem. Phys.* **1953**, *21*, 836.
- (57) Weaver, M. J. *Chem. Rev.* **1992**, *92*, 463.
- (58) Stackelberg, M.; Stracke, W. Z. *Electrochem.* **1949**, *53*, 118.
- (59) *CRC Handbook of Organic Photochemistry*; Scaiano, J. C., Ed.; CRC Press, Inc.: Boca Raton, FL, 1989; Vol. II, p 365.
- (60) Suppan, P. *J. Chem. Soc., Faraday Trans. 1* **1986**, *82*, 509.
- (61) Castano, F.; Lombrana, S.; Martinez, E.; Martinez, M. T. *Spectrosc. Lett.* **1983**, *16*, 805.
- (62) Lakowicz, J. R.; Zelent, B.; Kuśba, J.; Gryczynski, I. *J. Fluoresc.*, in press.
- (63) Edward, J. T. *J. Chem. Educ.* **1970**, *47*, 261.
- (64) Suppan, P. *Top. Curr. Chem.* **1992**, *163*, 95.
- (65) Eads, D. D.; Dismar, B. G.; Fleming, G. R. *J. Chem. Phys.* **1990**, *93* (2), 1136.
- (66) Kuśba, J.; Sipp, B. *Chem. Phys.* **1988**, *124*, 223.
- (67) Kuśba, J.; Lakowicz, J. R. In *Methods in Enzymology, Numerical Computer Methods*; Johnson, M. L., Brand, L., Eds.; Academic Press, Inc.: New York, 1994; Vol. 240, Part B, p 216.
- (68) Kuśba, J.; Sipp, B. *J. Lumin.* **1985**, *33*, 255.
- (69) Beechem, J. M.; Gratton, E.; Ameloot, M.; Knutson, J. R.; Brand, L. In *Topics in Fluorescence Spectroscopy, Volume 2: Principles*; Lakowicz, J. R., Ed.; Plenum Press: New York, 1991; p 241.
- (70) Bevington, P. R., Ed. *Data Reduction and Error Analysis for the Physical Sciences*; McGraw-Hill: New York, 1969; p 336.

JP9618688